

Published in final edited form as:

Nat Cell Biol. 2018 September ; 20(9): 1043–1051. doi:10.1038/s41556-018-0150-z.

Decrease in Plasma Membrane Tension Triggers PtdIns(4,5)P₂ Phase Separation to Inactivate TORC2

Margot Riggi^{#1,2,3,4}, Karolina Niewola-Staszewska^{#1,4}, Nicolas Chiaruttini², Adai Colom^{2,4}, Beata Kusmider¹, Vincent Mercier^{2,4}, Saeideh Soleimanpour^{4,5}, Michael Stahl¹, Stefan Matile^{4,5}, Aurélien Roux^{#2,4,*}, and Robbie Loewith^{#1,3,4,*}

¹Department of Molecular Biology, University of Geneva, Geneva 1211, Switzerland ²Department of Biochemistry, University of Geneva, Geneva 1211, Switzerland ³IGE3 Institute of Genetics and Genomics of Geneva, Geneva 1211, Switzerland ⁴Swiss National Centre for Competence in Research Program Chemical Biology, Geneva 1211, Switzerland ⁵Department of Organic Chemistry, University of Geneva, Geneva 1211, Switzerland

These authors contributed equally to this work.

Abstract

The Target of Rapamycin Complex 2 (TORC2) plays a key role in maintaining the homeostasis of plasma membrane (PM) tension. TORC2 activation upon increased PM tension involves redistribution of the Slm1 and 2 paralogs from PM invaginations known as eisosomes into membrane compartments containing TORC2. How Slm1/2 relocalization is triggered, and if/how this plays a role in TORC2 inactivation upon decreased PM tension is unknown. Using osmotic shocks and Palmitoylcarnitine (PalmC) as orthogonal tools to manipulate PM tension, we demonstrate that decreased PM tension triggers spontaneous, energy-independent reorganization of pre-existing phosphatidylinositol 4,5-bisphosphate (PtdIns(4,5)P₂) into discrete invaginated membrane domains which cluster and inactivate TORC2. These results demonstrate that an increase and a decrease in membrane tension are sensed through different mechanisms and highlight a role for membrane lipid phase separation in mechanotransduction.

Users may view, print, copy, and download text and data-mine the content in such documents, for the purposes of academic research, subject always to the full Conditions of use:http://www.nature.com/authors/editorial_policies/license.html#terms

*Correspondence and requests for materials should be addressed to Robbie Loewith: robbie.loewith@unige.ch or Aurélien Roux: aurelien.roux@unige.ch.

Data Availability

Data that support the findings of this study are available from the corresponding authors upon reasonable request.

Data Availability

Source data for Figures 1-6 and Supplementary Figures 1, 2, 5 and 6 have been provided as Supplementary Table 3. All other data that support the findings of this study are available from the corresponding authors upon reasonable request.

Author Contributions

M.R. and K. N.-S. carried out most of the experiments, with the exception of the GUV experiments (N.C.), Electron Microscopy experiments (B.K., V.M.), and the screening campaign that led to the identification of PalmC (F.G., M.S.). S.S. and S.M. designed and synthesized the FliptR probe, whose properties were characterized by A.C. M.R., K. N.-S., A.R. and R.L. designed experiments, interpreted results, and wrote the manuscript with contributions from all authors.

The authors declare no competing interest.

The plasma membrane (PM) is fundamental for cell survival. Not only does it form a selectively permeable barrier and dynamic interface, but it also serves as a scaffolding platform on which many fate-determining signaling decisions are taken. Furthermore, PM tension, defined as the in-plane counteracting force to surface expansion, plays an important role in transferring and integrating information in cells and within tissues 1–3. Biological membranes are constantly affected by processes - for example endo/exocytosis and cell migration - that impinge on their surface area, composition, and the activity of attachment proteins. This adds complexity but also provides the cell with multiple options for regulation of PM tension. Indeed, all cell types react, albeit with different kinetics, to counteract perturbations in PM tension suggesting that this is a tightly-controlled biophysical parameter 4–6.

Despite its established importance, little is known about the mechanisms by which PM tension is sensed and regulated. We recently identified the Target Of Rapamycin Complex 2 (TORC2) as a regulator of cell surface area and PM tension homeostasis 7. Specifically, we found that manipulations that presumably increase PM tension, including mechanical stretch of the PM, inhibition of sphingolipid biosynthesis and hypo-osmotic shock, all trigger the redistribution of the Slm proteins away from furrow-like invaginations organized by BAR protein assemblies called eisosomes 8,9, into Membrane Compartments Containing TORC2 (MCTs) 10. The signal that triggers Slm protein relocalization remains mysterious but membrane stretch has been reported to similarly induce mTORC2 signaling in mammalian cells 11, implying that TORC2 activation by increased PM tension is conserved. Our model does not consider what happens in the case of a decrease in PM tension, although one might assume that Slm1/2 would relocalize away from MCTs and back into eisosomes, inactivating TORC2. Here, we describe a small-molecule modulator of TORC2 signaling, Palmitoylcarnitine (PalmC), which acts primarily by reducing PM tension, monitored in live yeast cells with a mechanosensitive probe. Using PalmC and hyper-osmotic shocks as orthogonal approaches to diminish membrane tension, we found that neither treatment acutely affects Slm1 localization while both induce the phase separation of pre-existing PtdIns(4,5)P₂ into pronounced PM invaginations sequestering TORC2 and leading to its inactivation.

Results

TORC2 senses hypo- and hyperosmotic stress through independent mechanisms

Slm1 and 2 have previously been implicated in TORC2 signaling 12,13 and specifically in the perception of an increase in PM tension upstream of TORC2 7. In exponentially growing cells, ~60% of the Slm proteins localize to punctate PM protein assemblies called eisosomes 8,14 with the remainder in MCTs. Upon increased tension, the eisosomal pool relocalizes to MCTs and TORC2 signaling is increased 7. To further explore the molecular mechanisms regulating TORC2 activity, we applied osmotic shocks to single cells expressing Slm1-GFP and Lsp1-mCherry, which marks eisosomes. Changes in the colocalization between the two markers were compared with the evolution of TORC2 activity, assessed by monitoring the phosphorylation status of the direct TORC2 substrate T⁶⁶² in Ypk1 15,16. Consistent with our previous work 7, upon a hypo-osmotic shock, Slm1-GFP moved out of eisosomes and

TORC2 was activated with similar kinetics (Fig. 1a-c). However, although TORC2 activity was inhibited under a hyper-osmotic shock, both *Slm1*-GFP and *Lsp1*-mCherry distributions remained unaffected (Fig. 1d-f). We noted that hypo-osmotic shock transiently stimulated TORC2 activity in an amplitude-dependent manner, but that TORC2 activity went back to steady-state levels after only 5min, regardless of the amplitude of the shock that was applied to the cells (Supplementary Fig. S1a and S1c, left panel). Hyper-osmotic shock also caused a transient and amplitude-dependent inhibition of TORC2 activity, but in this case, the return of TORC2 activity to its basal level was slower and amplitude-dependent (Supplementary Fig. S1b and S1c, right panel). Together, these results demonstrate that hypo- and hyper-osmotic shocks are sensed upstream of TORC2 by distinct molecular mechanisms.

The HOG pathway 17,18 and the CWI pathway 19 constitute obvious candidates to couple osmotic stress to TORC2. However, cells deficient in single or multiple components in these pathways including: HOG pathway mutants *sln1 pbs2*, *hkr1 msb2* and *sln1 pbs2 hkr1 msb2*; a CWI pathway mutant *wsc1 mid2*; and, a combined mutant *wsc1 mid2 hkr1 msb2* (we were unable to recover a *wsc1 mid2 sln1 pbs2* quadruple mutant from our dissections) - all retained the ability to regulate TORC2 activity upon osmotic shocks similarly to WT cells (Supplementary Fig. S1d). Thus, the osmo-sensor(s) upstream of TORC2 must be independent of these factors.

TORC2 signaling affects PM tension

We entertained the idea that PM tension *per se* might be what is sensed upstream of TORC2. Hypo- and hyper-osmotic shocks are assumed to increase and decrease PM tension by increasing and decreasing turgor pressure respectively. To verify that osmotic shocks can be used to manipulate PM tension in yeast, we used the recently-developed mechanosensitive “FlipR” (Fluorescent LIPid Tension Reporter) probe 20 (Supplementary Fig. S2a). This twisted push-pull fluorophore stably integrates into the PM of cells where its planarization and polarization, and thus its fluorescence properties, are sensitive to mechanical forces acting on the membrane (Supplementary Fig. S2b). Specifically, its fluorescence lifetime, which can be determined by Fluorescence Lifetime Imaging Microscopy (FLIM), changes linearly with PM tension in model membranes and in mammalian cells (unpublished data), making it a valuable tool to monitor PM tension changes *in situ*. Consistently, hypo- and hyper-osmotic shocks to yeast cells respectively triggered an increase and a decrease in the FlipR lifetime, proportional to the intensity of the shock (Fig. 2a). This confirms that such shocks can be used to manipulate PM tension in yeast and that the FlipR probe can be used to qualitatively report on changes in PM tension.

We had previously proposed that TORC2 is part of a homeostatic feedback loop that maintains PM tension 7. The FlipR probe now allows us to test this model directly. We chose to inhibit TORC2 using a recently described chemical-genetic approach 21 wherein TORC2, but not TORC1, is specifically inhibited by rapamycin-FKBP12. Rapamycin-treatment of these cells caused a progressive increase in the lifetime of the fluorophore (Fig. 2b), indicating an increase in PM tension. Conversely, enhanced TORC2 signaling in a strain expressing a hyperactive *YPK2* allele 16 lowered PM tension, evidenced by a reduced

lifetime of the fluorophore (Fig. 2c). Together, these data add strong support to the model that TORC2 works in a functional feedback loop to maintain PM tensile homeostasis.

Palmitoylcarnitine (PalmC), a small-molecule tool to inhibit TORC2 and manipulate PM tension

In parallel to these studies, we had launched a high-throughput screening campaign to identify small molecules that specifically interfere with TOR signaling in *WT* yeast cells (described in methods, Supplementary Fig. S3a-b, Supplementary Tables 4-5). This effort revealed that Palmitoylcarnitine (PalmC, Supplementary Fig. S3c) is an inhibitor of TORC2, but not TORC1, signaling. Specifically, our screen revealed that the toxicity of PalmC is reduced in cells expressing hyperactive *YPK2* (Supplementary Fig. S3d). As this allele suppresses the lethality of TORC2 mutants, this result suggested that PalmC is toxic specifically because it interferes with TORC2 signaling. Consistently, treatment of cells with PalmC induced a fast, transient and dose-dependent inhibition of TORC2 activity, but not TORC1 activity, assessed by monitoring the TORC1-specific hydrophobic motif phosphorylation of Sch9 22 (Fig. 3a, b). Inclusion of PalmC in *in vitro* kinase assays had no effect on TORC2 kinase activity (Fig. 3c) suggesting that it targets a factor upstream of TORC2. Sensors of the HOG and CWI pathways were again dispensable for the response of TORC2 to PalmC (Supplementary Fig. S3e), and Hog1 was not activated by PalmC treatment (Supplementary Fig. S3f), suggesting that these pathways are not implicated in PalmC mode of action.

Based on the amphiphilic properties of PalmC we hypothesized that its effects could be due to modification of the biophysical properties of the PM, particularly tension. Consistent with this idea, we observed a fast and dramatic decrease in the lifetime of the FlptR probe after PalmC treatment (Fig. 3d), demonstrating that the drug induces a decrease in PM tension. If this is the cause of TORC2 inhibition, we would expect that hypo-osmotic shock would suppress this inhibition. To test this prediction, we used *fps1* cells that cannot efficiently export the osmo-protectant glycerol and thus are slow to recover from hypo-osmotic shock 23. Simultaneous application of a hypo-osmotic shock to these cells largely negated PalmC-induced TORC2 inactivation (Fig. 3e), while hyper-osmotic shock displayed an additive effect with PalmC on TORC2 inhibition (Supplementary Fig. S3g). We hypothesize that PalmC decreases PM tension by directly intercalating into the PM. Consistently, injecting PalmC into the buffer bathing Giant Unilamellar Vesicles (GUVs) resulted in a rapid increase in surface area of the GUV, evidenced by a fast elongation of the aspiration tongue into the micropipette holding the GUV (Fig. 3f). Blockage of exocytosis in *sec18^{ts}* cells 24, or endocytosis in Latrunculin A-treated cells, did not affect PalmC-induced decrease in Ypk1 T⁶⁶² phosphorylation (Supplementary Fig. S3h, i), suggesting that PalmC does not impinge on TORC2 signaling through either of these processes.

Based on these results, we decided to use PalmC as a tool, orthogonal to hyper-osmotic shock, to investigate the molecular mechanisms of TORC2 activity regulation upon decreases in PM tension.

A decrease in PM tension leads to the clustering of TORC2 to PtdIns(4,5)P₂-Enriched PM Domains

We first investigated the effect of a PalmC-induced decrease in PM tension on TORC2 localization. As previously observed¹⁰, TORC2, visualized through a GFP tag fused to its Avo3 subunit, localized to many small foci distributed along the PM. Following PalmC-treatment these foci clustered into fewer, brighter puncta (Fig. 4a). We measured and plotted the size distributions of these fluorescence maxima for untreated and PalmC-treated cells and found that they had very little overlap. This allowed us to define a fluorescent intensity threshold that separates small foci from larger puncta (Supplementary Fig. S4a). Puncta become noticeable after a few minutes of treatment, crested in number after 30min, when they were present in 84% of the cells, and persisted for up to 90min. The size, as well as the kinetics of the assembly and disassembly of these structures was dose-dependent. Notably, this timing correlated with both the kinetics of inhibition and reactivation of TORC2 activity and with a decrease and increase in PM tension as readout by the FliptR probe (Fig. 4b). Thus, TORC2 clustering into puncta is correlated with its inactivation.

Decreasing PM tension with a hyper-osmotic shock mimicked the PalmC effect and triggered TORC2 puncta formation, however direct inhibition of TORC2 activity by the ATP-competitive small molecule NVP-BHS34525 did not (Supplementary Fig. S4b). Together, these results suggest that clustering into puncta is potentially the cause of TORC2 inactivation in response to a decrease in PM tension, and not a consequence of its inactivation.

As with hyper-osmotic shock, the cellular distribution of Slm1-mCherry remained largely unaffected during the first 20 min after PalmC treatment, but these proteins then also began to cluster (Fig. 4c). We used the same threshold method to quantify Slm1 puncta (Supplementary Fig. S4c) and observed that they crested after 60min of treatment. Interestingly, the kinetics of Slm1 puncta formation tracks with the kinetics of TORC2 reactivation (Fig. 4b). Inhibition of TORC2 results in an increase in PM tension (Fig. 2b), and we assume that once cells have restored a sufficient amount of tension in the PM, the Slm proteins re-associate with TORC2 leading to its reactivation and the dissociation of the TORC2 puncta. Consistent with this model, anchoring of Slm1 to eisosomes during PalmC recovery prevented TORC2 reactivation (Supplementary Fig. S4d, e).

TORC2 is recruited to the PM *via* the PH domain of its Avo1 subunit which binds PtdIns(4,5)P₂¹⁰. Also, *tor2* mutants interact genetically with *MSS4*²⁶ which encodes the sole PtdIns(4)P-5-kinase in yeast. Thus, we speculated that decreased PM tension might affect the cellular distribution of this lipid, in turn affecting TORC2 activity. To investigate this, we examined the cellular distribution of PtdIns(4,5)P₂ using the biosensor GFP-2xPH^{PLCδ}²⁷. In basal conditions, PtdIns(4,5)P₂ was distributed uniformly along the PM, in accordance with previous studies²⁸. Upon PalmC treatment or hyperosmotic shock, we observed a fast and striking redistribution of GFP-2xPH^{PLCδ} at the PM, whereas direct inhibition of TORC2 did not trigger this lipid rearrangement (Fig. 4d). Staining cells expressing the GFP-2xPH^{PLCδ} biosensor with FM4-64 showed that the clusters appearing upon decreased PM tension are truly enriched in PtdIns(4,5)P₂, as evidenced by the ratiometric comparison of the images acquired in the two channels (Fig. 4e). These

“PtdIns(4,5)P₂-Enriched-Structures” (PES) quickly disassemble upon PM stretching induced by a hypo-osmotic shock (Fig. 4f), further supporting the idea that a decreased PM tension constitutes the primary cause of their formation.

PM buckling into large invaginations has been observed when cells possess an excess of PM, for example, after hyper-osmotic shock 29. Interestingly, PalmC-treated, but not control cells, presented large folded PM invaginations, enriched in PtdIns(4,5)P₂, when observed by electron microscopy after anti-GFP immunogold labelling in cells expressing the PtdIns(4,5)P₂ biosensor (Supplementary Fig. S4f). Similar structures were previously observed in cells deleted for the genes encoding inositol-5-phosphatases, and thus contain elevated levels of PtdIns(4,5)P₂ 30. These structures are reminiscent of failed endocytic events 31; however, endocytosis requires an intact actin cytoskeleton in yeast 31, and pretreatment with Latrunculin A (LatA), an actin depolymerizing agent, did not prevent PES formation (Supplementary Fig. S3g). Additionally, LatA treatment did not affect PES dissolution, implying that endocytosis is not essential to resolve these structures (Supplementary Fig. S4h).

As TORC2 clusters and PES appear after PalmC treatment with similar kinetics we asked whether or not these structures are related; indeed, we found that Avo3-GFP and mCherry-2xPH^{PLC6} puncta colocalized (Fig. 4g, 60.3±14.6% colocalization). Together, these results suggest that the relocalization and clustering of TORC2 into PES is part of a common mechanism to transiently inhibit TORC2 activity upon a decrease of PM tension. At later time points, Slm1-mCherry puncta also colocalized with PES (Fig. 4h, 65.4±10.4% colocalization), likely to reactivate TORC2 as described above.

PtdIns(4,5)P₂ is crucial for TORC2 clustering and inhibition upon a decrease in PM tension

We postulated that the interaction between the PH domain of Avo1 and PtdIns(4,5)P₂ constitutes the driving mechanism responsible for TORC2 clustering. Both localization and activity of TORC2 are lost upon the shift of thermosensitive *mss4-103* cells to non-permissive temperature (Supplementary Fig. S5a-b). To prevent the detachment of TORC2 from the PM upon loss of PtdIns(4,5)P₂ we replaced the PH domain of Avo1 with a CAAX motif, to enable the PtdIns(4,5)P₂-independent, yet fully functional, PM recruitment of TORC2 10. The localization of TORC2^{CAAX} in *mss4-103* cells was assessed at the permissive (30°C) and the non-permissive (37°C) temperatures, before and after PalmC treatment. At the permissive temperature, TORC2^{CAAX} behaved similarly to TORC2^{WT} – it localized to small foci before PalmC treatment and to large puncta after treatment, but it failed to cluster at the non-permissive temperature (Fig. 5a). Growth at 37°C *per se* did not alter the PalmC-induced relocalization of TORC2. These observations demonstrate that PtdIns(4,5)P₂ is necessary for TORC2 clustering upon PalmC treatment in a manner that does not solely involve the PH domain of Avo1.

We next queried whether the remodeling of the PM itself upon PalmC treatment was also PtdIns(4,5)P₂-dependent. The absence of PtdIns(4,5)P₂ in *mss4-103 TORC2^{CAAX}* cells grown at 37°C precluded the use of the GFP-2xPH^{PLC6} biosensor so, for these experiments, changes in the PM structure were visualized using FM4-64. At the permissive temperature, in both *WT* and *mss4-103 TORC2^{CAAX}* cells, FM4-64 puncta appeared upon PalmC

treatment and colocalized with PES (Fig. 5b). FM4-64 clusters were not observed in *mss4-103 TORC2^{CAAX}* cells upon PalmC treatment at the restrictive temperature (Fig. 5b), demonstrating that PtdIns(4,5)P₂ is required for the remodeling of the PM that follows a decrease in PM tension. Furthermore, although the basal activity of the TORC2^{CAAX} variant is relatively low in *mss4-103* cells (Supplementary Fig. S5c), this remaining activity is largely resistant to PalmC treatment when cells are incubated at the non-permissive temperature (Fig. 5c). This indicates that PtdIns(4,5)P₂-mediated TORC2 clustering is necessary for TORC2 inhibition. Yeast cells growing in the wild must respond to stresses that affect plasma membrane tension such as osmotic shock and we wondered if TORC2 inactivation contributes to the ability of cells to tolerate such stresses. To test this, we queried if depletion of PtdIns(4,5)P₂ would affect the ability of cells to survive and/or recover from stresses that trigger acute loss of PM tension. Indeed, inactivation of *mss4-103*, but not the temperature shift *per se*, impaired regrowth following transient PalmC exposure or hyper-osmotic shock (Fig. 5d and Supplementary Fig. S5d). These observations indicate that PtdIns(4,5)P₂ is a crucial intermediate in the sensing of decreased PM tension upstream of TORC2, and that inhibition of TORC2 signaling is an essential response of cells experiencing a sudden decrease in PM tension.

A decrease in PM tension triggers PtdIns(4,5)P₂ phase separation

Quantification of GFP-2xPH^{PLC6} signal after PalmC treatment shows PtdIns(4,5)P₂ clustering into distinct puncta, but no global increase in PtdIns(4,5)P₂ (Supplementary Fig. S6a and b). Mss4 co-localizes to PalmC-induced PES, cresting at 15 min and disappearing by 90 min (Fig. 6a), suggesting that decreased PM tension might act through Mss4 to create PES.

To challenge this hypothesis, we tested whether PES would still form in ATP-depleted cells, in which PtdIns(4,5)P₂ synthesis cannot occur. Upon ATP-depletion, PtdIns(4,5)P₂ is rapidly turned over through the action of several phosphatases (Inp51, 52 and 53) and the GFP-2xPH^{PLC6} biosensor disassociates from the PM within a minute (Fig. 6b, top panel). Deletion of *INP51* and *INP52* prevents this loss of PtdIns(4,5)P₂. Remarkably, even after ATP depletion, PalmC treatment still rapidly induces the formation of PES in *inp51 inp52* cells (Fig. 6b, bottom panel). These results demonstrate that decreased PM tension triggers PES formation *via* a redistribution of pre-existing PtdIns(4,5)P₂ and not *via de novo* synthesis. PtdIns(4,5)P₂ present within PES is not selectively shielded from phosphatases since the GFP-2XPH^{PLC6} probe is also rapidly relocalized from PES to the cytosol upon ATP depletion in *WT*, but not *inp51 inp52* cells (Supplementary Fig. S6c). From these results we conclude that Mss4 relocalization ensures that PtdIns(4,5)P₂ levels remain high in PES while PM tension is low and that ATP depletion *per se* does not trigger PES disassembly.

Finally, we wondered whether the formation of PES could be due to a lipid phase separation within the PM. To assess this, we used the lipophilic dye Laurdan and subsequent calculation of the Generalized Polarization (GP) as a readout for lipid order^{32,33}. Laurdan partitions equally into liquid-disordered (Ld) or liquid-ordered (Lo) membranes and is not associated to specific lipids, so GP values reflect the overall organization of the PM³⁴, being

high in Lo phases, and low in Ld phases. The pixel histogram obtained from the GP images of untreated PM followed a normal distribution, meaning that the PM globally displays a homogeneous organization (Fig. 6c). After PalmC treatment, we observed the appearance of a second population of pixels displaying higher GP (Fig. 6c), indicating the presence of a more ordered phase. Using cells expressing the mCherry variant of the PtdIns(4,5)P₂ biosensor, we confirmed that the domains of high GP correspond to PES (Fig. 6d). Moreover, we observed the appearance of high-GP puncta upon PalmC treatment in ATP-depleted *inp51 inp52*, but not *WT*, cells (Fig. 6e). This confirms the necessity of PtdIns(4,5)P₂ in the phase separation process. Endocytic BAR domain proteins such as Rvs161 or its dimerization partner Rvs167, could conceivably drive lipid phase separation. However, this seems unlikely as Rvs167-GFP does not redistribute to PES upon decreased PM tension (Supplementary Fig. S6d). Collectively, our results support the model that PES formation is the result of a spontaneous phase separation of PtdIns(4,5)P₂.

Discussion

We propose that the respective inactivation and activation of TORC2 upon decrease and increase in membrane tension are regulated through fundamentally different mechanisms (Fig. 6f). Sensing of *increased* PM tension involves the translocation of Slm proteins from eisosomes to MCTs where they activate TORC2 ⁷. Here, we demonstrated that *decreased* PM tension triggers a spontaneous, energy-independent PtdIns(4,5)P₂ phase separation into discrete invaginated membrane domains which cluster and inactivate TORC2. Recently, we reported that clustering of TORC1 upon glucose starvation is both necessary and sufficient for its inactivation ³⁵. Cryo-electron microscopy revealed that TORC1 clusters are actually a giant helix of regularly assembled TORC1 dimers, organized such that the kinase active site is physically occluded and thus not accessible to substrate. Given the structural similarities between TORC1 and TORC2 ³⁶, we anticipate that the TORC2 clusters that we report here will represent an analogous, higher-order TORC2 assembly responsible for its inactivation.

This result presents the interesting possibility that PtdIns(4,5)P₂ phase separation is the primary molecular sensor of decreased PM tension. PtdIns(4,5)P₂ patches are well suited to pattern the localized events required for the regulation of a given signaling pathway, by recruiting and activating a range of effector proteins. For example, PES-like structures have also been observed in higher eukaryotes, where they function to organize CD44-Ezrin interactions linking the PM to the cytoskeletal actin network ³⁷, and to promote exocytosis by concentrating SNARE proteins ^{38,39}. Interestingly, local PtdIns(3,4)P₂ production upon growth factor deprivation was very recently implicated in the inhibition of mTORC1 residing on lysosomes and late endosomes ⁴⁰. Collectively, these observations suggest that protein sorting by lipid phase-separation could constitute a currently underappreciated mechanism of signal transduction regulation in general and regulation of TOR signaling in particular.

Methods

Yeast strains and plasmids

All strains and plasmids used in this study are listed in Supplementary Tables 1 and 2. Yeast strains were generated either by homologous recombination of PCR-generated fragments as previously described or by crossing, sporulation and subsequent dissection of the spores. All primers used for the generation of the strains are listed in Supplementary Table 6. Strains were confirmed by PCR and sequencing. Cloning and site-directed mutagenesis were performed following standard procedures and plasmids were verified by sequencing. All tagged proteins are functional and expressed from their endogenous promoter.

Yeast culture

Yeast cells were grown according to standard procedures at 30°C or 37°C as indicated in either YPD or SC medium lacking appropriate amino acids required for plasmid selection to an OD₆₀₀ of 0.6–0.8. For the hypo-osmotic shocks, cells were grown to OD₆₀₀ = 0.8 in SC containing 1 M of sorbitol, which was then diluted to the indicated sorbitol concentrations by addition of pre-warmed SC medium. For the hyper-osmotic shocks, cells were grown to OD₆₀₀ = 0.6 in SC media, before adding the appropriate volume of SC+2M sorbitol to reach the desired final sorbitol concentration.

Chemicals and drugs

Rapamycin (LC Laboratories) was dissolved in 90% ethanol, 10% Tween® 20 at 1mg/mL and used at a final concentration of 200nM. Wortmannin (LC Laboratories) was dissolved in DMSO at 5mg/mL and used at a final concentration of 2µM. Cycloheximide (Sigma) was dissolved in H₂O at 10mg/mL and used at 2µg/mL. NVP-BHS345 (Novartis) was dissolved in DMSO at 10mM and used at a final concentration of 10µM. Palmitoylcarnitine was dissolved in DMSO at 10mM and used at 10µM, unless otherwise stated. The FLipTR probe, dissolved in DMSO 20, was used at a final concentration of 2ng/mL. The Laurdan dye (6-Dodecanoyl-2-dimethylaminonaphthalene) was maintained as a 2.5mM stock solution in DMF and used at 2.5µM. The FMTM4-64 dye ((N-(3-Triethylammoniumpropyl)-4-(6-(4-(Diethylamino) Phenyl) Hexatrienyl) Pyridinium Dibromide, Thermofisher) was dissolved at 10mM in DMSO and used at a final concentration of 10µM. For ATP depletion, cells were treated for 10min with a combination of 3mM NaN₃ and 50mM 2-deoxy-D-glucose 41.

High-throughput drug screen

Both TORC1 and TORC2 perform essential functions which can be genetically bypassed upon introduction of mutations that constitutively activate downstream effector pathways 42. Specifically, the lethality caused by loss of TORC1 activity can be suppressed by simultaneous expression of a constitutively active variant of the Sch9 kinase and deletion of *TIP41* which encodes a protein phosphatase regulator 43; lethality associated with the loss of TORC2 activity is suppressed by expression of a hyperactive variant of the Ypk2 kinase 16. To identify small molecules that potentially interfere with TORC1 and/or TORC2 signaling we screened 89,850 molecules from the Rockefeller HTSRC compound library 44

and sought out compounds that are more toxic to *WT* than to bypass cells (Supplementary Fig. S3a-b, Supplementary Table 4). A total of 89,850 unique compounds from The Rockefeller University High Throughput and Spectroscopy Resource Center library were screened. They were part of the following commercially available libraries: ChemDiv (San Diego, CA), Cerep (Poitiers, France), ChemBridge (San Diego, CA), AMRI (Albany, NY), Greenpharma (Orléans, France), BioFocus (Charles River, Wilmington, MA), Prestwick Chemical (San Diego, CA) and LOPAC (Sigma, Carlsbad, CA). Compounds stocks were stored in a total of 281 384-well polypropylene plates at a final concentration of 5mM in DMSO at -30°C.

10µL of Agar Yeast Extract-Peptone-Dextrose (YPD) broth was preloaded into each well of clear-bottomed 384-well assay plates using a Thermo Multidrop Combi dispenser (Thermo Scientific). Compounds stock plates were thawed at room temperature, and 0.1µL of compound was added to the wells of the assay plates using a Perkin Elmer Janus equipped with a Perkin Elmer Nanohead. The overnight, saturated cultures of *WT* (TB50 MATa *leu2-3,112 ura3-52 rme1 trp1 his3*) and of the TORC1/2 bypass strain (MS119; TB50a *pRS304::SCH9^{DE} tip41 ::HphMX pRS303::YPK2^{D239A}*) were diluted to OD₆₀₀=0.125 in YPD. 40µL of both diluted cultures were dispensed into the wells of parallel assay plates to achieve a final concentration of compounds of 10µM and a final concentration of DMSO of 0.2%. Plates were subsequently incubated at 30°C in a humidified bag for 24h without agitation. 2 µg/mL of Cycloheximide, which inhibits the growth of both strains, was kept in 8 wells in column 24 and used as a positive control. 0.2% DMSO was kept in the column 23 and used as a negative control. Rapamycin, which inhibits the growth of the *WT* but not the double bypass (BY) strain, was used at a final concentration of 1µg/mL as an internal control for selectivity in the 8 remaining wells of column 24.

The absorbance at 600nm was measured for both strains using a plate reader (Perkin Elmer Envision) before (T_0) and after 24h incubation (T_{24}). The normalized percentage inhibition of yeast growth (NPI) was calculated for each sample as follows:

$$NPI = (x - \mu^-) / (\mu^+ - \mu^-) \times 100$$

where x is the sample (OD₆₀₀ T_{24} - OD₆₀₀ T_0), μ^- is the negative control mean and μ^+ is the positive control mean.

55 compounds (listed in Supplementary Table 5) with $NPI_{WT} - NPI_{BY} > 20\%$ or $NPI_{WT} - NPI_{BY} < -50\%$ were selected for retesting in concentration response experiments to determine half maximal inhibitory concentrations (IC₅₀). These compounds were serially diluted by half for a total of 10 dilutions to achieve an assay concentration ranging from 30µM to 0.06µM. PalmC, which initially displayed toxicity specifically to the bypass strain, was amongst these 55 compounds (highlighted in yellow in Supplementary Table 5).

Spot Assays

Strains were grown overnight at 30°C, diluted to $OD_{600}=0.1$, grown to exponential phase and diluted to $OD_{600}=0.3$. 3 μ L of 1/5 serial dilutions were spotted on plates containing the appropriate treatment. The plates were photographed after incubation at 30°C for 2-3 days.

Antibodies

The following antibodies were used in this study: goat anti-Ypk1 1:1000 (Cell Signaling, not produced anymore); mouse anti-phospho-Ypk1-T⁶⁶² 1:500 7; rabbit anti-phospho-Sch9-T⁷³⁷ 1:250 45; rabbit anti-Sch9 1:10000 21; rabbit anti-phospho-p38 T¹⁸⁰/T¹⁸² 1:1000 (Cell Signaling 9211S); rabbit anti-Hog1 1:1000 (Santa Cruz Technology sc-9079); and the appropriate infrared dye-coupled secondary antibodies used at a dilution of 1:10000 (Alexa Fluor 680-conjugated anti-mouse 926-68072 and anti-rabbit 926-68073 secondary antibodies from LI-COR Biosciences and IRDye® 800 conjugated anti-goat 605-732-125 secondary antibody from Rockland Bioconcept).

TCA Protein Extraction & Phosphoproteins Immunodetection

6% TCA was directly added to exponentially growing yeast cultures and cells were incubated for 5 min on ice before collection. Extracts were prepared as described previously 43 and proteins were resolved on a 7.5% SDS gel and blotted on a nitrocellulose membrane. Immunodetection was performed using the indicated antibodies and the Odyssey® IR imaging system (LI-COR Biosciences).

In vitro kinase assay

GST-Ypk1^{K376A} and TORC2 were purified from yeast as previously described 21. TORC2 was pre-incubated with the appropriate concentrations of 1 μ L of drug/vehicle for 10min at 25°C in a thermomixer rotating at 800rpm. The kinase reactions were started by the addition of 5 μ g of Ypk1^{K376A}, 300 μ M ATP, 4.2mM MgCl₂ and 100 μ Ci gamma-³²P ATP. They were incubated for 10min at 30°C in a thermomixer rotating at 800rpm, and terminated with the addition of 6x SDS-PAGE sample buffer and a 10min incubation at 65°C. Samples were separated by SDS-PAGE on 10% gels, stained with Sypro Ruby Protein gel stain and analyzed using a BioRad Molecular Imager.

Fluorescence Microscopy

Cells were grown at 30°C in SC medium to $OD_{600} = 0.6$, mounted on coverslips coated with Concanavalin A (Sigma) and immediately imaged with a spinning-disc microscope assembled by 3i (Intelligent Imaging Innovation, Denver, USA) and Nikon (Eclipse C1, Nikon, Tokyo, Japan) using a 100 x objective (NA=1.3, Nikon). Laurdan dye integrated into cell membranes was excited along the 405 nm laser line and emission read at 430~470 nm (representing the liquid ordered phase) or 490~550 nm (representing the liquid disordered phase). For microfluidics experiments, a Concanavalin A-coated coverslip was bonded to the bottom surface of a flow chamber (sticky-slide VI 0.4, Ibidi, Munich, Germany) with one entry connected to a syringe pump (Aladdin, World Precision Instrument, Sarasota, USA) and the other left open for sequential introduction of different solutions. The flow chamber was primed with SC medium prior to the loading of cells. Loaded cells were washed several

times with SC medium, and then subjected to the appropriate treatments. Images were taken as either single focal planes or captured as Z-series to generate 2D maximum intensity projections. For FLIM (Fluorescence Lifetime Imaging Microscopy), cells were grown overnight in SC medium to $OD_{600} = 0.05$ to 0.1 , concentrated by spinning and incubated for 1min with 2ng/mL of the FLipTR probe before imaging using the SymPhoTime 64 software.

Electron Microscopy

Fixed cells (2,5% glutaraldehyde in phosphate buffer 0.1M for 2h) were further treated with 2% osmium tetroxide and immersed in a solution of uranyl acetate 0.25% overnight. The pellets were dehydrated in increasing concentrations of ethanol followed by pure propylene oxide, then embedded in Epon resin. Thin sections were stained with uranyl acetate and lead citrate and observed in a Tecnai 20 EM.

Image processing and quantification

For quantification of the colocalization of fluorescent markers, (Fig. 1a, 1d, 4g, 4h), z-stacks of cells were recorded and deconvoluted. The same threshold was used for each channel in all tested conditions to create binary images. Binary masks were overlaid to an RGB image and yellow (colocalizing marker; ≥ 4 pixels) and green (non-colocalizing; ≥ 4 pixels) foci were counted using the ImageJ plug-in Cell Counter (National Institutes of Health, <http://www.macbiophotonics.ca/imagej/>). The percentage of foci containing colocalizing markers was calculated with Excel (Microsoft).

Ratiometric images (Fig. 4e) were constructed using the image calculator tool from ImageJ.

Quantification of protein foci intensities (Fig. S4a and S4c) was performed using ImageJ.

For FLIM analysis (Fig. 2, 3d, 4b), we used the SymPhoTime 64 software to fit the data according to a 2-exponential reconvolution model and calculate the lifetime of the FLipTR probe.

To study the evolution of PtdIns(4,5)P₂ concentration (Fig. S6a), single focal plane images of the cell middle were taken, a 2px-wide line was drawn around the cortex of cells using ImageJ, and fluorescence intensity values were plotted for each channel. For quantification of cellular total GFP-2xPH^{PLCδ} fluorescence intensity (Fig. S6b), 0.5μm-spaced Z-planes series of cells were taken under identical laser power and exposure time. The cytoplasmic mean fluorescence intensity was subtracted from the total cellular fluorescence intensity (both measured using ImageJ) for each focal plane before adding the obtained values.

Generalized Polarization (GP) values (Fig. 6c) were calculated for each pixel of a yeast PM according to the following equation:

$$GP = (I_{440} - I_{490}) / (I_{440} + I_{490})$$

where I_{440} and I_{490} represents the intensity of pixels in the areas of interest in the image acquired in the ordered and disordered spectral channels, respectively.

Statistics and reproducibility

The samples sizes and statistical tests were selected based on previous studies with similar methodologies. All experiments were repeated at least three times, giving similar results. The results of independent experiments are presented as mean values; error bars represent the SD, or the propagated error when the value of each experiment was itself calculated as a mean of individual cells. Statistical significance was tested using the two-tailed Student's t-test.

Supplementary Material

Refer to Web version on PubMed Central for supplementary material.

Acknowledgements

The authors thank Guillaume Molinard and Manoel Prouteau for technical help and Tarun Kapoor, Jeanne Chiaravalli and J. Fraser Glickman for their collaboration on the HTS campaign. M.R. acknowledges the iGE3 PhD Student Awards. R.L. acknowledges support from the Canton of Geneva, project funding from the Swiss National Science Foundation (SNSF) and the European Research Council Consolidator grant program. AR acknowledges funding from the Swiss National Fund for Research Grants N°31003A_130520, N°31003A_149975 and N°31003A_173087, and the European Research Council Starting Grant N° 311536 (2011 call). M.R., K.N.S., A.C., S.S., S.M., A.R. and R.L. are greatly indebted to the National Centre for Competence in Research in Chemical Biology for its support.

References

1. Paluch E, Heisenberg CP. Biology and physics of cell shape changes in development. *Curr Biol*. 2009; 19:R790–799. DOI: 10.1016/j.cub.2009.07.029 [PubMed: 19906581]
2. Yu H, Mouw JK, Weaver VM. Forcing form and function: biomechanical regulation of tumor evolution. *Trends in Cell Biology*. 2011; 21:47–56. DOI: 10.1016/j.tcb.2010.08.015 [PubMed: 20870407]
3. Diz-Munoz A, Fletcher DA, Weiner OD. Use the force: membrane tension as an organizer of cell shape and motility. *Trends Cell Biol*. 2013; 23:47–53. DOI: 10.1016/j.tcb.2012.09.006 [PubMed: 23122885]
4. Dai J, Sheetz MP. Mechanical properties of neuronal growth cone membranes studied by tether formation with laser optical tweezers. *Biophys J*. 1995; 68:988–996. DOI: 10.1016/S0006-3495(95)80274-2 [PubMed: 7756561]
5. Lieber AD, Yehudai-Resheff S, Barnhart EL, Theriot JA, Keren K. Membrane tension in rapidly moving cells is determined by cytoskeletal forces. *Curr Biol*. 2013; 23:1409–1417. DOI: 10.1016/j.cub.2013.05.063 [PubMed: 23831292]
6. Morris CE, Homann U. Cell surface area regulation and membrane tension. *J Membr Biol*. 2001; 179:79–102. [PubMed: 11220366]
7. Berchtold D, et al. Plasma membrane stress induces relocalization of Slm proteins and activation of TORC2 to promote sphingolipid synthesis. *Nat Cell Biol*. 2012; 14:542–547. DOI: 10.1038/ncb2480 [PubMed: 22504275]
8. Walther TC, et al. Eisosomes mark static sites of endocytosis. *Nature*. 2006; 439:998–1003. DOI: 10.1038/nature04472 [PubMed: 16496001]
9. Olivera-Couto A, Aguilar PS. Eisosomes and plasma membrane organization. *Mol Genet Genomics*. 2012; 287:607–620. DOI: 10.1007/s00438-012-0706-8 [PubMed: 22797686]
10. Berchtold D, Walther TC. TORC2 plasma membrane localization is essential for cell viability and restricted to a distinct domain. *Mol Biol Cell*. 2009; 20:1565–1575. DOI: 10.1091/mbc.E08-10-1001 [PubMed: 19144819]

11. Diz-Munoz A, et al. Membrane Tension Acts Through PLD2 and mTORC2 to Limit Actin Network Assembly During Neutrophil Migration. *PLoS Biol.* 2016; 14:e1002474.doi: 10.1371/journal.pbio.1002474 [PubMed: 27280401]
12. Fadri M, Daquinag A, Wang S, Xue T, Kunz J. The pleckstrin homology domain proteins Slm1 and Slm2 are required for actin cytoskeleton organization in yeast and bind phosphatidylinositol-4,5-bisphosphate and TORC2. *Mol Biol Cell.* 2005; 16:1883–1900. DOI: 10.1091/mbc.E04-07-0564 [PubMed: 15689497]
13. Tabuchi M, Audhya A, Parsons AB, Boone C, Emr SD. The phosphatidylinositol 4,5-bisphosphate and TORC2 binding proteins Slm1 and Slm2 function in sphingolipid regulation. *Mol Cell Biol.* 2006; 26:5861–5875. DOI: 10.1128/MCB.02403-05 [PubMed: 16847337]
14. Grossmann G, et al. Plasma membrane microdomains regulate turnover of transport proteins in yeast. *J Cell Biol.* 2008; 183:1075–1088. DOI: 10.1083/jcb.200806035 [PubMed: 19064668]
15. Aronova S, et al. Regulation of ceramide biosynthesis by TOR complex 2. *Cell Metab.* 2008; 7:148–158. DOI: 10.1016/j.cmet.2007.11.015 [PubMed: 18249174]
16. Kamada Y, et al. Tor2 directly phosphorylates the AGC kinase Ypk2 to regulate actin polarization. *Mol Cell Biol.* 2005; 25:7239–7248. DOI: 10.1128/MCB.25.16.7239-7248.2005 [PubMed: 16055732]
17. Hohmann S. Control of high osmolarity signalling in the yeast *Saccharomyces cerevisiae*. *FEBS Lett.* 2009; 583:4025–4029. DOI: 10.1016/j.febslet.2009.10.069 [PubMed: 19878680]
18. Brewster JL, Gustin MC. Hog1: 20 years of discovery and impact. *Sci Signal.* 2014; 7:re7.doi: 10.1126/scisignal.2005458 [PubMed: 25227612]
19. Levin DE. Regulation of cell wall biogenesis in *Saccharomyces cerevisiae*: the cell wall integrity signaling pathway. *Genetics.* 2011; 189:1145–1175. DOI: 10.1534/genetics.111.128264 [PubMed: 22174182]
20. Soleimanpour S, et al. Headgroup engineering in mechanosensitive membrane probes. *Chem Commun (Camb).* 2016; 52:14450–14453. DOI: 10.1039/c6cc08771j [PubMed: 27901525]
21. Gaubitz C, et al. Molecular Basis of the Rapamycin Insensitivity of Target Of Rapamycin Complex 2. *Mol Cell.* 2015; 58:977–988. DOI: 10.1016/j.molcel.2015.04.031 [PubMed: 26028537]
22. Urban J, et al. Sch9 is a major target of TORC1 in *Saccharomyces cerevisiae*. *Mol Cell.* 2007; 26:663–674. DOI: 10.1016/j.molcel.2007.04.020 [PubMed: 17560372]
23. Beese SE, Negishi T, Levin DE. Identification of positive regulators of the yeast *fps1* glycerol channel. *PLoS Genet.* 2009; 5:e1000738.doi: 10.1371/journal.pgen.1000738 [PubMed: 19956799]
24. Novick P, Ferro S, Schekman R. Order of events in the yeast secretory pathway. *Cell.* 1981; 25:461–469. [PubMed: 7026045]
25. Rispal D, et al. Target of Rapamycin Complex 2 Regulates Actin Polarization and Endocytosis via Multiple Pathways. *J Biol Chem.* 2015; 290:14963–14978. DOI: 10.1074/jbc.M114.627794 [PubMed: 25882841]
26. Desrivieres S, Cooke FT, Parker PJ, Hall MN. MSS4, a phosphatidylinositol-4-phosphate 5-kinase required for organization of the actin cytoskeleton in *Saccharomyces cerevisiae*. *J Biol Chem.* 1998; 273:15787–15793. [PubMed: 9624178]
27. Kavran JM, et al. Specificity and promiscuity in phosphoinositide binding by pleckstrin homology domains. *J Biol Chem.* 1998; 273:30497–30508. [PubMed: 9804818]
28. Stefan CJ, Audhya A, Emr SD. The yeast synaptojanin-like proteins control the cellular distribution of phosphatidylinositol (4,5)-bisphosphate. *Mol Biol Cell.* 2002; 13:542–557. DOI: 10.1091/mbc.01-10-0476 [PubMed: 11854411]
29. Dupont S, Beney L, Ritt JF, Lherminier J, Gervais P. Lateral reorganization of plasma membrane is involved in the yeast resistance to severe dehydration. *Biochim Biophys Acta.* 2010; 1798:975–985. DOI: 10.1016/j.bbamem.2010.01.015 [PubMed: 20116363]
30. Singer-Kruger B, Nemoto Y, Daniell L, Ferro-Novick S, De Camilli P. Synaptojanin family members are implicated in endocytic membrane traffic in yeast. *J Cell Sci.* 1998; 111(Pt 22):3347–3356. [PubMed: 9788876]
31. Stefan CJ, Padilla SM, Audhya A, Emr SD. The phosphoinositide phosphatase Sjl2 is recruited to cortical actin patches in the control of vesicle formation and fission during endocytosis. *Mol Cell Biol.* 2005; 25:2910–2923. DOI: 10.1128/MCB.25.8.2910-2923.2005 [PubMed: 15798181]

32. Owen DM, Williamson DJ, Magenau A, Gaus K. Sub-resolution lipid domains exist in the plasma membrane and regulate protein diffusion and distribution. *Nat Commun.* 2012; 3:1256.doi: 10.1038/ncomms2273 [PubMed: 23212385]
33. Sanchez SA, Tricerri MA, Gratton E. Laurdan generalized polarization fluctuations measures membrane packing micro-heterogeneity in vivo. *Proc Natl Acad Sci U S A.* 2012; 109:7314–7319. DOI: 10.1073/pnas.1118288109 [PubMed: 22529342]
34. Harris FM, Best KB, Bell JD. Use of laurdan fluorescence intensity and polarization to distinguish between changes in membrane fluidity and phospholipid order. *Biochim Biophys Acta.* 2002; 1565:123–128. [PubMed: 12225860]
35. Prouteau M, et al. TORC1 organized in inhibited domains (TOROIDS) regulate TORC1 activity. *Nature.* 2017; doi: 10.1038/nature24021
36. Karuppasamy M, et al. Cryo-EM structure of *Saccharomyces cerevisiae* target of rapamycin complex 2. *Nat Commun.* 2017; 8:1729.doi: 10.1038/s41467-017-01862-0 [PubMed: 29170376]
37. Chen X, et al. Phosphatidylinositol 4,5-bisphosphate clusters the cell adhesion molecule CD44 and assembles a specific CD44-Ezrin heterocomplex, as revealed by small angle neutron scattering. *J Biol Chem.* 2015; 290:6639–6652. DOI: 10.1074/jbc.M114.589523 [PubMed: 25572402]
38. Honigmann A, et al. Phosphatidylinositol 4,5-bisphosphate clusters act as molecular beacons for vesicle recruitment. *Nat Struct Mol Biol.* 2013; 20:679–686. DOI: 10.1038/nsmb.2570 [PubMed: 23665582]
39. van den Bogaart G, et al. Membrane protein sequestering by ionic protein-lipid interactions. *Nature.* 2011; 479:552–555. DOI: 10.1038/nature10545 [PubMed: 22020284]
40. Marat AL, et al. mTORC1 activity repression by late endosomal phosphatidylinositol 3,4-bisphosphate. *Science.* 2017; 356:968–972. DOI: 10.1126/science.aaf8310 [PubMed: 28572395]

Methods only References

41. Narita T, Naganuma T, Sase Y, Kihara A. Long-chain bases of sphingolipids are transported into cells via the acyl-CoA synthetases. *Sci Rep.* 2016; 6 25469. doi: 10.1038/srep25469
42. Loewith R, Hall MN. Target of rapamycin (TOR) in nutrient signaling and growth control. *Genetics.* 2011; 189:1177–1201. DOI: 10.1534/genetics.111.133363 [PubMed: 22174183]
43. Huber A, et al. Characterization of the rapamycin-sensitive phosphoproteome reveals that Sch9 is a central coordinator of protein synthesis. *Genes Dev.* 2009; 23:1929–1943. DOI: 10.1101/gad.532109 [PubMed: 19684113]
44. Vincent J, et al. Small molecule inhibition of cGAS reduces interferon expression in primary macrophages from autoimmune mice. *Nat Commun.* 2017; 8:750.doi: 10.1038/s41467-017-00833-9 [PubMed: 28963528]
45. Wanke V, et al. Caffeine extends yeast lifespan by targeting TORC1. *Mol Microbiol.* 2008; 69:277–285. DOI: 10.1111/j.1365-2958.2008.06292.x [PubMed: 18513215]

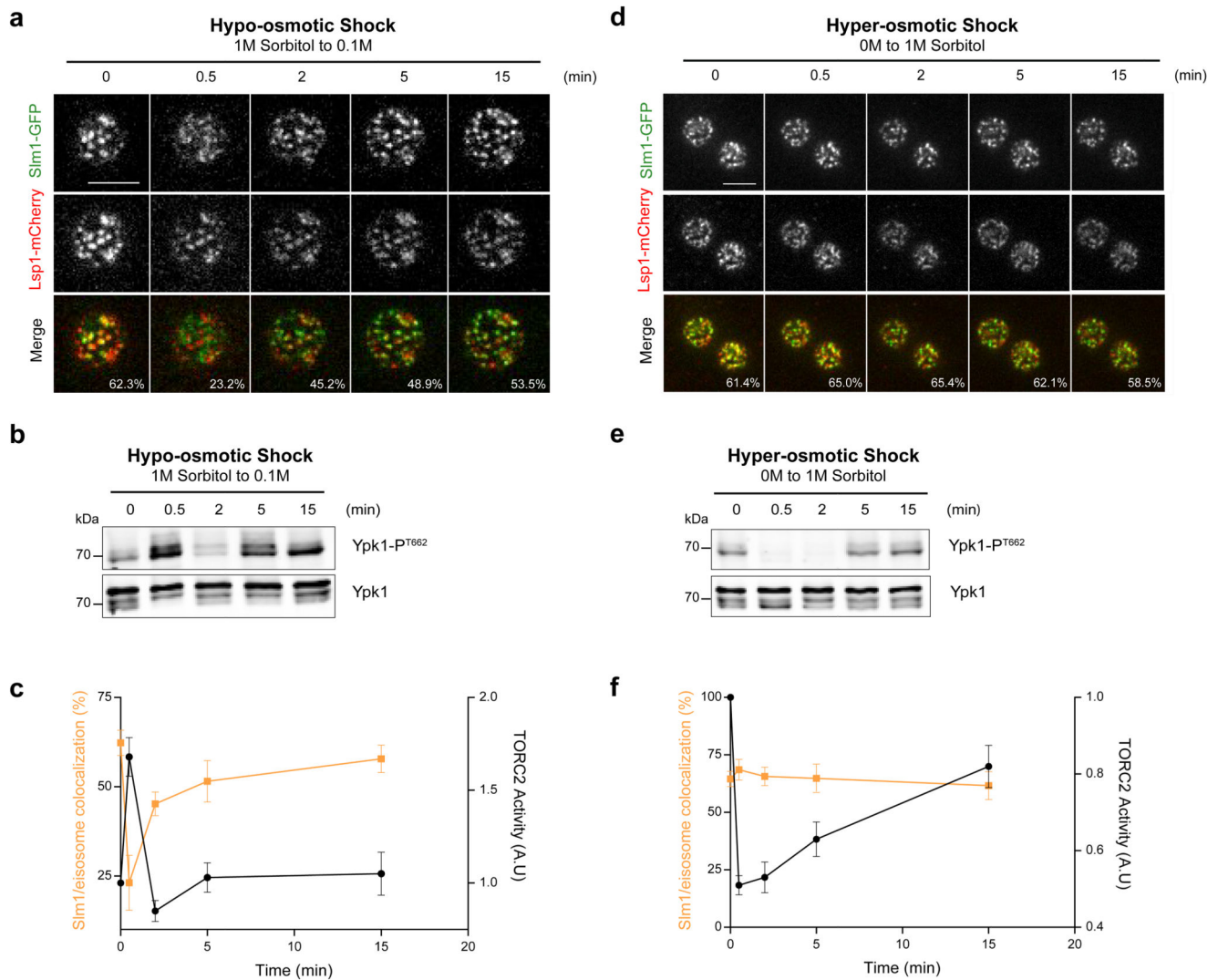


Fig. 1. TORC2 senses hypo- and hyper-osmotic shocks through different mechanisms. (a, d) Top section confocal images of cells expressing Slm1-GFP and Lsp1-mCherry following hypo- (a) or hyperosmotic shock (d). The percentage of colocalization between markers is indicated as the mean from $n > 30$ cells [$n = 34$ cells for hypo-osmotic shock and $n = 38$ for hyper-osmotic shock] pooled from three independent experiments. Scale bars, $5 \mu\text{m}$. (b, e) Hypo- (b) and hyper-osmotic shocks (e) respectively activate and inhibit TORC2 activity, assessed by monitoring Ypk1 T⁶⁶² phosphorylation. Presented blots are representative of results obtained in three independent experiments, and all unprocessed scans are shown in Supplementary Figure 7. (c, f) Correlation between Slm1-GFP/eisosome colocalization and TORC2 activity following hypo- (c) or hyperosmotic shock (f). Error bars represent the SD of mean values of three independent experiments concerning TORC2 activity, or the SD to the mean calculated from $n > 30$ [$n = 34$ cells for hypo-osmotic shock and $n = 38$ for hyper-osmotic shock] cells pooled from three independent experiments in the case of the colocalization between Slm1 and eisosomes. Source data are included in Supplementary Table 3.

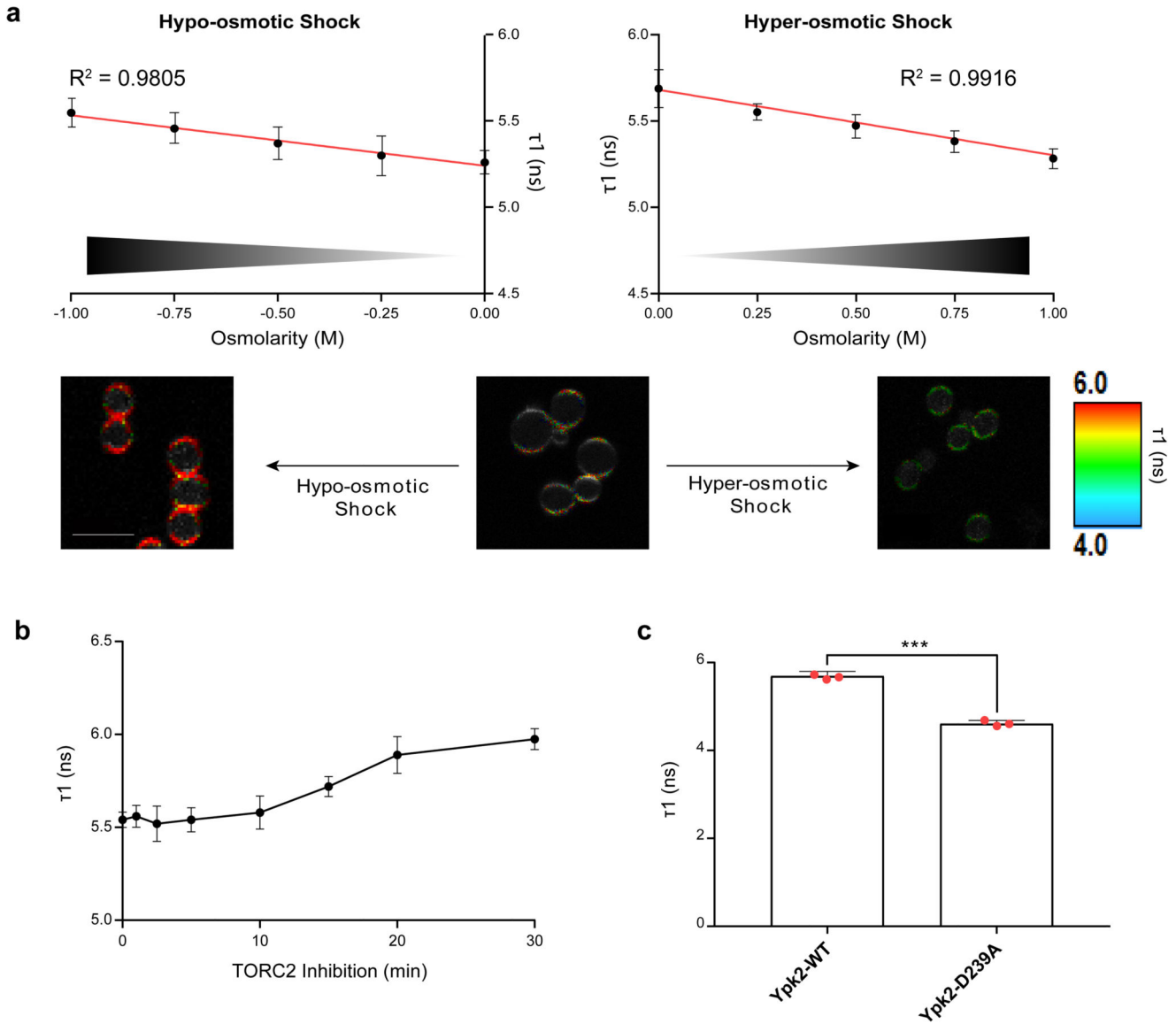


Fig. 2. TORC2 regulates PM tension in a homeostatic feedback loop manner. (a) Osmotic shocks impact PM tension in a dose-dependent, linear fashion. Cells were submitted to a range of osmotic shocks and the lifetime of the FLipTR (Fluorescent LIPid Tension Reporter) probe was determined by Fluorescence Lifetime Imaging Microscopy (FLIM). Note that different control values for the hyper- and hypo-osmotic shocks are due to the different initial growth conditions SC vs. SC + 1M sorbitol. Error bars represent the propagated error of mean values for three independent experiments (with n=20 cells). Scale bars, 5 μ m. (b) TORC2 inhibition results in increased PM tension. TORC2 was inhibited by Rapamycin in *TOR1-1 AVO3*¹²⁷⁴⁻¹⁴³⁰ cells 21, and the lifetime of the FLipTR probe was measured by FLIM, and presented as the mean +/- SD (n=20 cells). This experiment was repeated twice with similar results. (c) Elevated TORC2 signaling lowers PM tension. The lifetime of the FLipTR probe was measured by FLIM in cells expressing either a *WT* or a hyperactive version of *YPK2* 16 (*** p<0.001, two-tailed unpaired t-test, p=0.00014). Error

bars represent the propagated error of mean values for three independent experiments (with n=20 cells).

Source data are included in Supplementary Table 3.

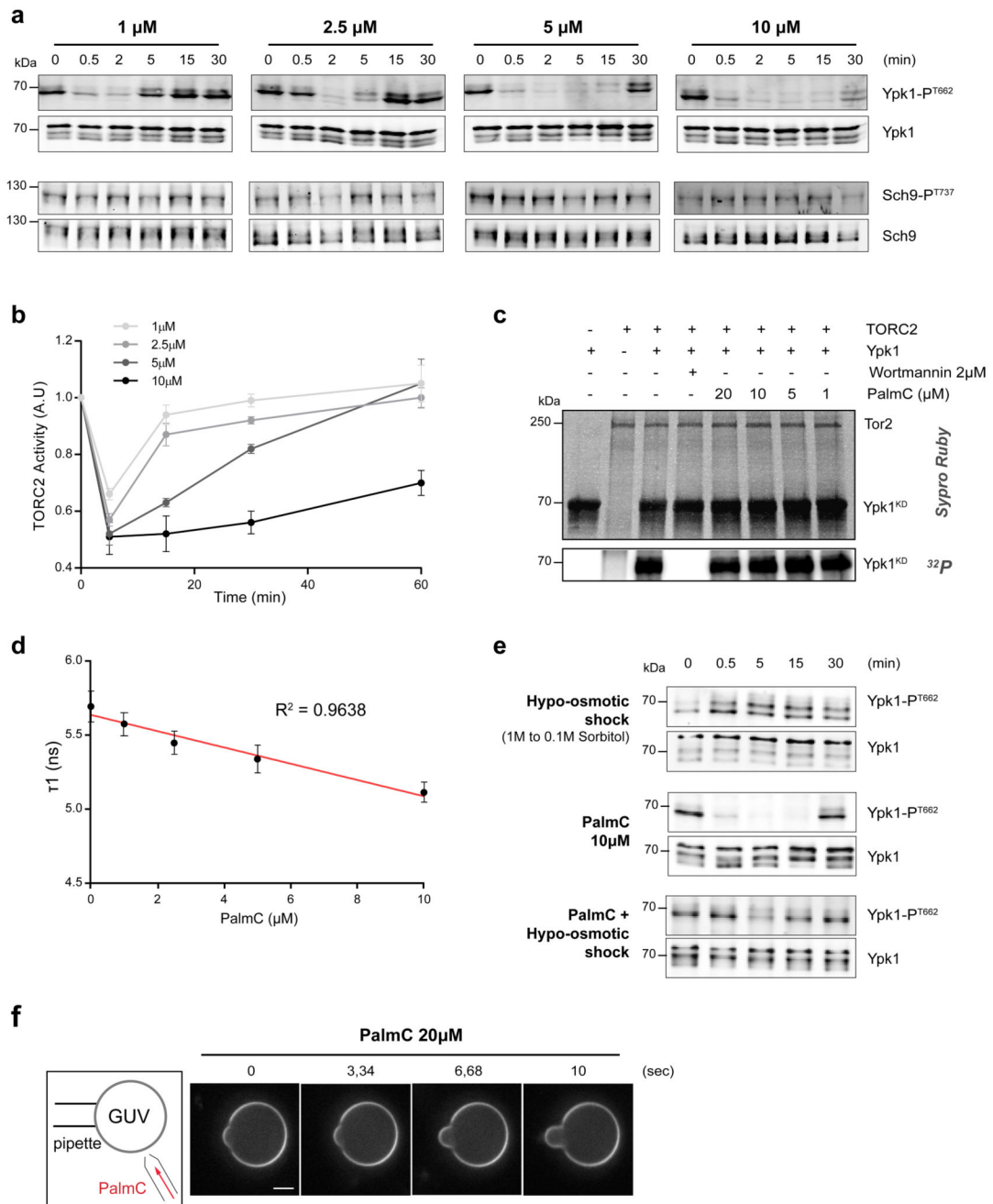


Fig. 3. Palmitoylcarnitine (PalmC) affects PM tension and TORC2 activity.

(a) PalmC inhibits TORC2, but not TORC1, in a time- and dose-dependent manner *in vivo*. Phosphorylation of Ypk1 T⁶⁶² and Sch9 T⁷³⁷ were monitored in PalmC-treated cells. Presented blots are representative of results obtained in three independent experiments. (b) Evolution of TORC2 activity after varying PalmC doses. Error bars represent the SD of mean values of three independent experiments. (c) PalmC does not inhibit TORC2 *in vitro*. Purified TORC2 was incubated with the indicated inhibitors, radiolabeled γ -ATP, and a kinase-dead version of Ypk1. After separation proteins were visualized by Sypro Ruby

staining and incorporation of radiolabeled ATP imaged with a phosphoimager. This experiment was repeated three times with similar results. **(d)** PalmC induces a decrease in PM tension. Cells incubated with the FLipTR probe were treated with PalmC and imaged after 5 min by FLIM. Error bars represent the propagated error of mean values for three independent experiments (n=20 cells). **(e)** Simultaneous increase in PM tension negates PalmC effects on TORC2 activity. Phosphorylation of Ypk1 T⁶⁶² was monitored in *fps1* cells treated with PalmC, +/- a hypo-osmotic shock, at the indicated time points. This experiment was repeated twice with similar results. **(f)** PalmC incorporates into membranes. Time-lapse following PalmC injection (20 μ M) in the vicinity of a Giant Unilamellar Vesicle (GUV). Additional membrane is evidenced by appearance of an aspiration tongue. This experiment was repeated twice with similar results.

All unprocessed scans of blots are shown in Supplementary Figure 7. Source data are included in Supplementary Table 3.

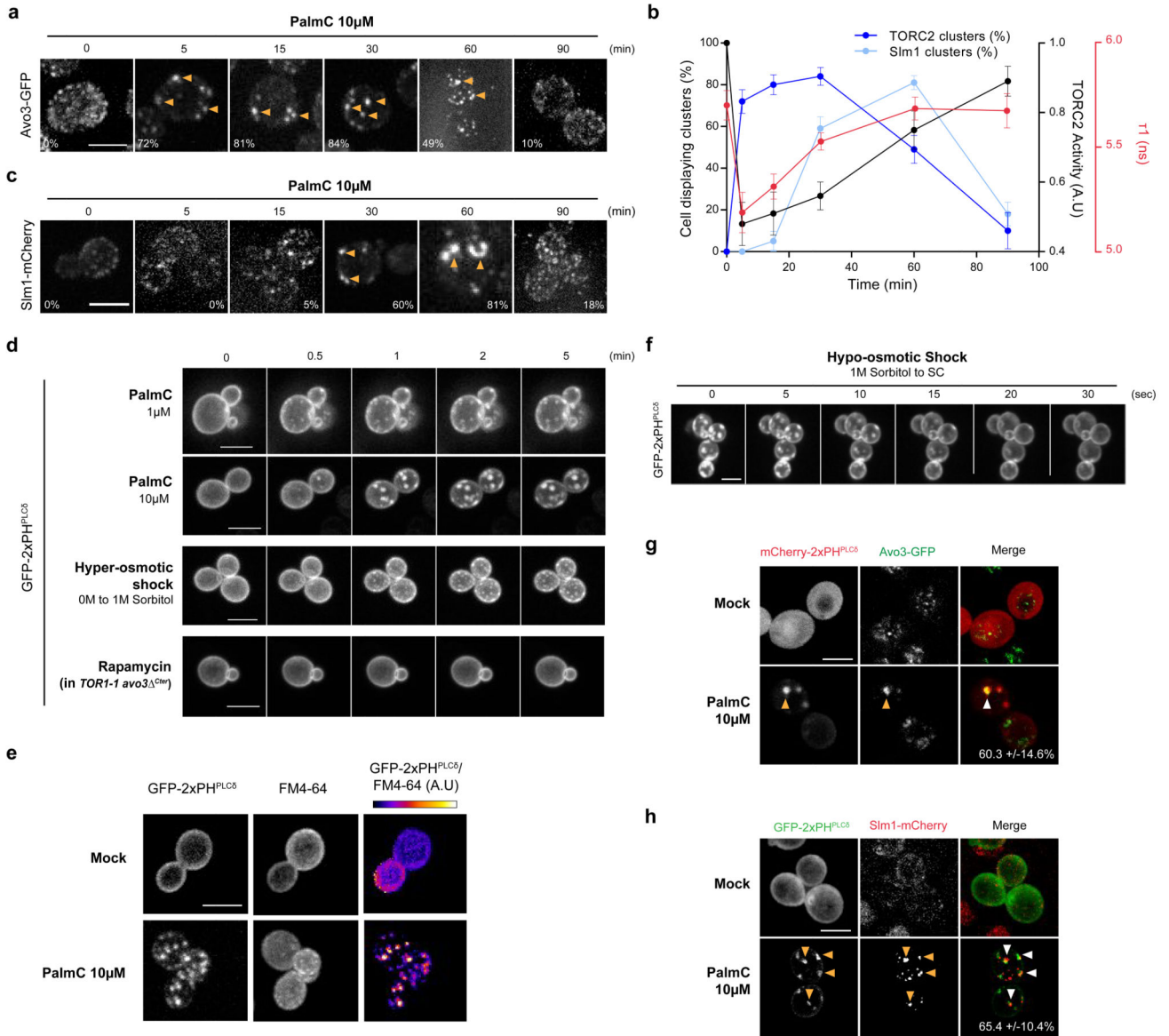


Fig. 4. Decreased PM tension causes TORC2 to cluster into PtdIns(4,5)P₂-Enriched-Structures (PES).

(a, c) PalmC induces rapid TORC2 (Avo3-GFP, (a)) and delayed Slm1-mCherry (c) clustering. The percentage of cells displaying clusters is indicated as the mean of three independent experiments including 50 cells. (b) Correlation of TORC2 clustering (dark blue), Slm1 clustering (light blue), TORC2 activity (black), and PM tension (red), following PalmC treatment. Clustering was assessed in three independent experiments, each including 50 cells. TORC2 activity was monitored by Ypk1 T⁶⁶² phosphorylation and the error bars represent the SD of three independent experiments. PM tension was monitored through the FLipTR probe lifetime and the error bars represent the propagated error of mean values of three independent experiments (n=20 cells). (d) A decrease in PM tension, but not direct inhibition of TORC2, triggers PtdIns(4,5)P₂ redistribution. Time lapse of cells expressing

the GFP-2xPH^{PLC δ} biosensor upon PalmC treatment, hyper-osmotic shock, or Rapamycin treatment. **(e)** The membrane domains formed upon decreased PM tension are enriched in PtdIns(4,5)P₂. Cells expressing the GFP-2xPH^{PLC δ} biosensor and labelled with FM4-64 were mock treated or treated with PalmC for 5 min. The last column presents the ratiometric images of the two channels, constructed using ImageJ image calculator tool. **(f)** An increase in PM tension induces fast disassembly of the PES. Time lapse of cells expressing the GFP-2xPH^{PLC δ} biosensor and pretreated with PalmC for 15 min upon a 1M hypo-osmotic shock. TORC2 **(g)** and Slm1 **(h)** clusters co-localize with PES after PalmC treatment. The percentage of colocalization between markers is the mean calculated from 10 cells pooled from two independent experiments, +/- SD.

All images are maximum projections of 0.5 μ m-spaced Z-planes of the cells, and representative of results obtained in at least two independent experiments. Scale bars, 5 μ m. Source data are included in Supplementary Table 3.

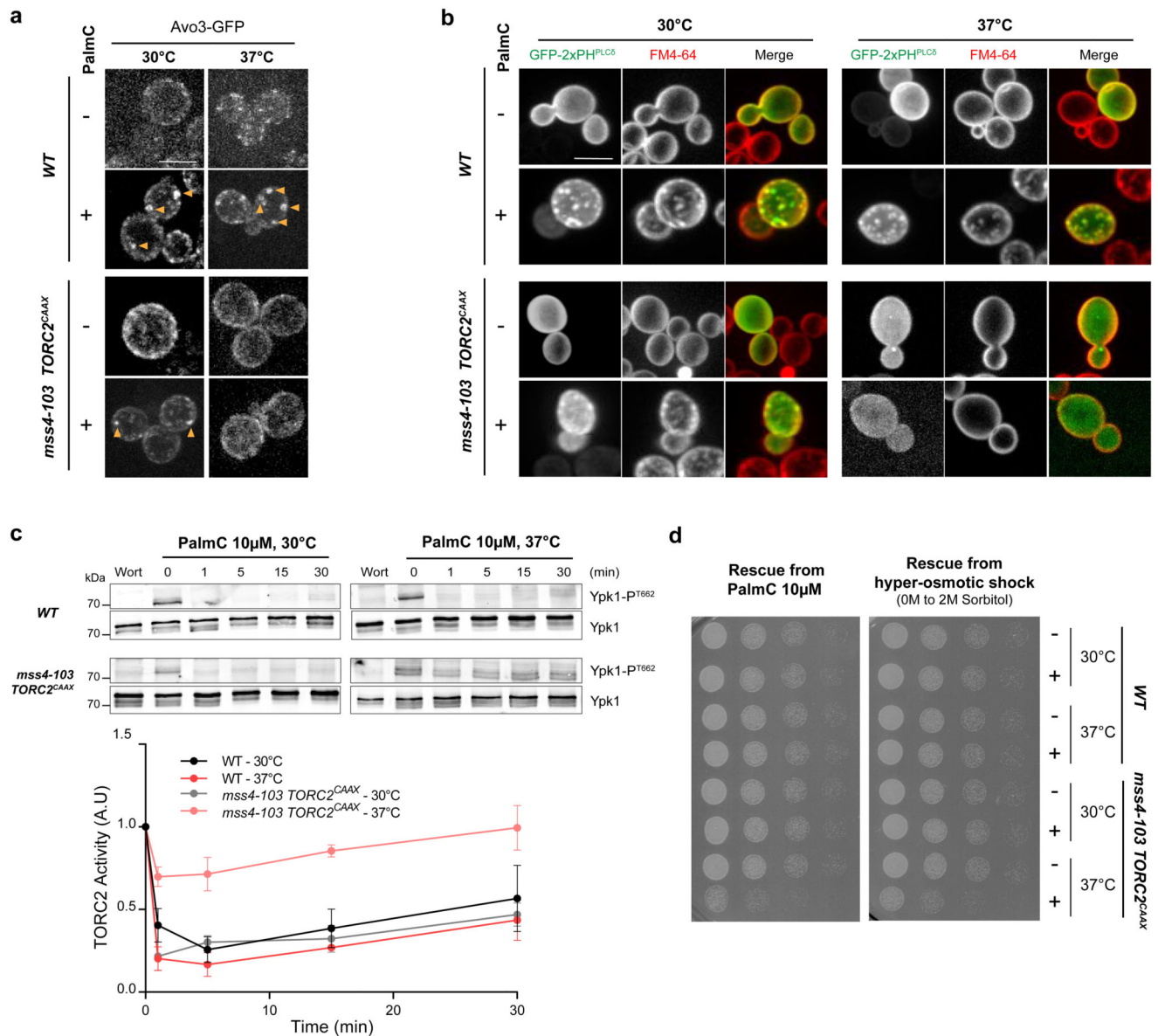


Fig. 5. PtdIns(4,5)P₂ is crucial for TORC2 inhibition and cell survival upon an acute decrease in PM tension.

(a) PtdIns(4,5)P₂ is required for TORC2 clustering upon decrease PM tension. Avo3-GFP localization upon PalmC treatment, in *WT* and *mss4-103 TORC2^{CAAX}* cells grown at the indicated temperatures for 90min. (b) PtdIns(4,5)P₂ is required for PM remodeling upon decreased PM tension. FM4-64 PM labeling in *WT* and *mss4-103 TORC2^{CAAX}* cells expressing GFP-2xPH^{PLC6} and grown at the indicated temperatures for 90min, upon PalmC treatment. (c) PtdIns(4,5)P₂ is required for TORC2 inhibition upon decrease PM tension. Evolution of Ypk1 T⁶⁶² phosphorylation upon PalmC or Wortmannin (Wort, 2μM, 5min) treatment, in *WT* and *mss4-103 TORC2^{CAAX}* cells grown at the indicated temperatures for 90min. Unprocessed scans of blots are shown in Supplementary Figure 7. Error bars represent the SD of mean values of three independent experiments, and source data are

included in Supplementary Table 3. **(d)** TORC2 inhibition is necessary for efficient survival of an acute decrease in PM tension. *WT* or *mss4-103* TORC2^{CAAX} cells were grown at the indicated temperature for 90min before being treated with 10 μ M PalmC for 60min or 2M Sorbitol for 15min. Serial dilutions were then spotted onto YPD plates and cell regrowth monitored 24h later.

All images are maximum projections of 0.5 μ m-spaced Z-planes of the cells, and representative of results obtained in at least three independent experiments. Scale bars, 5 μ m.

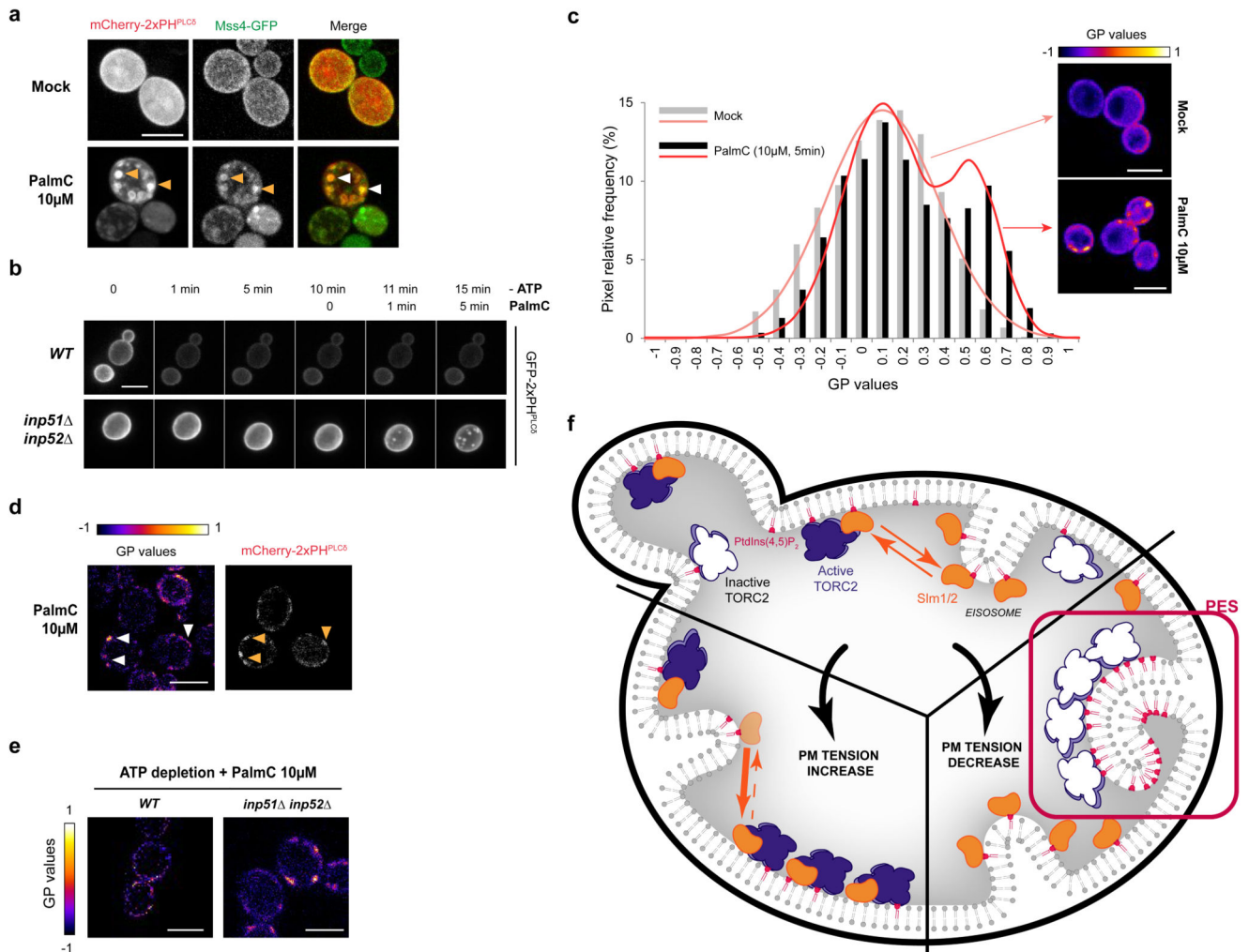


Fig. 6. PtdIns(4,5)P₂ redistributes through ATP-independent phase separation upon decreased PM tension

(a) Mss4-GFP relocates to PES upon decreased PM tension. Images are maximum projections of 0.5µm-spaced Z-planes of the cells. (b) Mss4 activity is not required for PES assembly. Time-lapse images of *WT* or *inp51 inp52* cells expressing the GFP-2xPH^{PLC6} biosensor upon ATP depletion followed by 10µM PalmC treatment. Images are maximum projections of 0.5µm-spaced Z-planes of the cells. (c) Decreased PM tension induces a lipid phase separation within the PM. PM pixel distribution and modeled distribution after Laurdan GP (Generalized Polarization) imaging of untreated and PalmC-treated cells (n=25 cells pooled from two independent experiments, >2250 pixels, n=2583 and 2251 pixels for the mock and PalmC conditions respectively). Representative color-coded GP images of the equatorial plan of the cells, constructed with ImageJ image calculator tool, are shown. Source data are included in Supplementary Table 3. (d) PM domains of higher GP correspond to PES. Cells expressing the mCherry-2xPH^{PLC6} biosensor were stained with the Laurdan dye after 5min of 10µM PalmC treatment, and a representative colour-coded GP image of the equatorial plan of the cells, constructed with ImageJ image calculator tool, is

shown. **(e)** ATP depletion prevents the formation of puncta of higher GP upon PalmC treatment in *WT*, but not in *inp51 inp52* cells. Representative colour-coded GP images of maximum projections of 0.5 μ m-spaced Z-planes of the cells, constructed with ImageJ image calculator tool, are shown. **(f)** Increased and decreased PM tension are sensed through different mechanisms by TORC2. Increased PM tension induces the translocation of Slm proteins (orange) from eisosomes to MCTs where they activate TORC2 (purple). Decreased PM tension triggers a spontaneous, energy-independent PtdIns(4,5)P₂ phase separation into invaginated membrane domains (PES) which cluster and inactivate TORC2 (white). All images are representative of results obtained in at least two independent experiments. Scale bars, 5 μ m.